The Meteoritical Society

Meteoritics & Planetary Science 44, Nr 4, 559–572 (2009)
Abstract available online at http://meteoritics.org

Nebular history of amoeboid olivine aggregates

N. SUGIURA[1*], M. I. PETAEV[2], M. KIMURA[3], A. MIYAZAKI[1], and H. HIYAGON[1]

[1]Department of Earth and Planetary Science, University of Tokyo, 7-3-1, Hongo, Bunkyo-ku, Tokyo, Japan
[2]Harvard-Smithsonian Center for Astrophysics and Department of Earth and Planetary Sciences, Harvard University, 20 Oxford Street, Cambridge, Massachusetts 02138, USA
[3]Faculty of Science, Ibaraki University, Mito 310-8512, Japan
[*]Corresponding author. E-mail sugiura@eps.s.u-tokyo.ac.jp

(Received 17 July 2008; revision accepted 14 December 2008)

Abstract–Minor element (Ca, Cr, and Mn) concentrations in amoeboid olivine aggregates (AOAs) from primitive chondrites were measured and compared with those predicted by equilibrium condensation in the solar nebula. CaO concentrations in forsterite are low, particularly in porous aggregates. A plausible explanation appears that an equilibrium Ca activity was not maintained during the olivine condensation. CaO and MnO in forsterite are negatively correlated, with CaO being higher in compact aggregates. This suggests that the compact aggregates formed either by a prolonged reheating of the porous aggregates or by condensation and aggregation of forsterite during a very slow cooling in the nebula.

INTRODUCTION

Amoeboid olivine aggregates (AOAs) are olivine-rich objects that condensed and accreted in the solar nebula. AOAs are considered to be related to Ca-Al-rich inclusions because of similar oxygen isotopic compositions (Hiyagon and Hashimoto 1999). Although there are many studies of AOAs (e.g., Krot et al. 2004c; Weisberg et al. 2004) unresolved issues still remain, such as how AOA olivine condensed and how accretion of AOAs occurred. We are particularly interested in condensation processes of AOAs' forsterite grains because recent advances in condensation calculations suggest that concentrations of minor elements in forsterite can be used to learn how the condensation process proceeded (Petaev et al. 2005). According to the equilibrium condensation calculations, forsterite condensation starts at 1370 K in a 10^{-4} bar solar nebula of solar composition. Initially, the forsterite is expected to be Ca-rich, but as temperature decreases it would become progressively richer in relatively volatile minor elements (Mn, Cr, and Fe) and depleted in Ca, if equilibrium is maintained (see below for details). However, because a long time is needed for equilibration in solid phases, equilibrium cannot be maintained below closure temperatures (Dodson 1973) which depend on the grain size, the diffusion rates of elements in olivine, and the nebular cooling rate.

Since almost all Ca has condensed prior to forsterite condensation and because Ca diffusion in forsterite is slow, Ca is the element that should show clear signature of disequilibrium in forsterite. Most Mn and Cr are expected to condense after practically all forsterite has condensed. Hence they should reveal thermal history at lower temperatures (<1250 K). Since the forsterite grain size can be estimated, and diffusion rates in forsterite are fairly well known, cooling rates during condensation may be estimated based on minor element concentrations in AOAs.

However, minor element (Ca, Mn, Cr, and Fe) concentrations in olivine are affected by many factors: 1) total nebular pressure and/or dust enrichment relative to the solar composition, 2) redox conditions that mainly affect Fe and Cr concentrations, 3) deviations from equilibrium which depend strongly on cooling rates, 4) reheating in the solar nebula which is known to have affected some AOAs (Komatsu et al. 2001), and 5) metamorphism in the parent body (Chizmadia et al. 2002).

Here we report concentrations of minor elements in AOA forsterite from primitive chondrites. The minor element concentrations are compared with those predicted by thermodynamic calculations of forsterite condensation. With the aid of petrographic features of AOAs and diffusion data of Ca, Mn and Cr in forsterite, the thermal history of AOAs in the nebula is examined quantitatively.

SAMPLES AND EXPERIMENTAL METHODS

Sixteen AOAs from Acfer 094 (ungrouped, type 3.00), 4 AOAs from Yamato (Y-) 81020 (CO3.05), and one AOA each from Allan Hills (ALH) 77307 (CO3.03) and Murchison

(CM2) were studied in detail. These chondrites are considered to be most primitive (Grossman and Brearley 2005; Kimura et al. 2008). Concentrations of major and minor elements (Al, Mg, Si, Ca, Ti, V, Cr, Mn, Fe, and Ni) in forsterite were measured either by an energy dispersive spectrometer attached to a scanning electron microscope (SEM-EDS), or by wavelength dispersive spectrometers of an electron microprobe (EPMA). The EPMA analyses were conducted at 15 kV and a sample current of 80 nA. The counting times are 20 s for Mg, 30 for Si, Ca, Ti, Cr and Fe, and 40 for Al, V, Mn and Ni. The standard ZAF matrix correction method was used. The detection limits of EPMA analyses in this study are 0.05 wt% for NiO, 0.03 wt% for CrO and MnO, 0.02 wt% for Al_2O_3, TiO_2 and V_2O_3 and 0.01 wt% for CaO. All the reported data except for a fine-grained AOA in Murchison were obtained by EPMA.

Cathodoluminescence (CL) color images were taken with a Mini CL detector (Gatan Inc.) attached to the SEM. RGB color filters were attached in front of the detector window to get color-filtered images. The blue, green, and red filters transmit light of wave lengths 370 nm to 510 nm, 510 nm to 600 nm, and longer than 600 nm, respectively. At longer wave lengths (>800 nm), the sensitivity of the CL detector itself rather than the filter transmission limits the CL detection. Color images were produced by superposing the RGB-filtered images using the Adobe Photoshop software.

Equilibrium condensation calculations at a total pressure of 10^{-4} bar were performed to explore how minor element concentrations in olivine change during condensation. The calculation procedure is similar to that described in Petaev and Wood (2005) and the details will be published elsewhere.

RESULTS

Figures 1a and 1c show typical porous and compact AOAs, respectively. Compact AOAs tend to show pinkish CL (Fig. 1d, at least in the interior) whereas porous AOAs tend to show reddish CL. The reddish CL (Fig. 1b) color is caused by small amounts of Mn (and/or Cr) in forsterite whereas pinkish CL is considered to be emitted from lattice defects (Steele 1988; Benstock et al. 1997). The presence of Mn and Cr in red-CL forsterites and near absence of these elements in pink-CL forsterite were confirmed by the EMPA analyses that will be discussed shortly. Compact AOAs are more abundant in Y-81020 than in the other meteorites. Figure 1e shows a very porous, fine-grained AOA in Murchison. The typical grain size is ~2 μm. The fine-grained nature suggests that this is probably a very primitive aggregate. Nevertheless, several triple junctions are present, suggesting that the AOA experienced some sintering after aggregation. The minor element concentrations (determined by EDS), which cannot be very precise because of the fine grain-size, high porosity and tilted surfaces of crystals, are CaO ~ 0.09 wt%, CrO ~ 0.09 wt% and MnO ~ 0.24 wt%, which are typical for the porous AOAs in Y-81020 and Acfer 094. Note, that ^{16}O-rich micron-sized olivine grains (not aggregates) have been found in the matrix of Vigarano (Kunihiro et al. 2005). Fine-grained AOAs similar to that shown in Fig. 1e have not been widely recognized, possibly because they are fragile and easily destroyed during preparation of polished sections. They must have formed by aggregation of fine olivine grains. Therefore, the presence of fine olivine grains in the matrix of primitive chondrites (Kunihiro et al. 2005) suggests that fine-grained AOAs may be more ubiquitous than we recognize. The presence of such olivine grains is also important because it suggests that the original olivine grain size was of the order of 1 μm. Figure 1f shows the interior of an AOA from ALH 77307. It consists of forsterite, metal, diopside, diffuse gray areas (halos) and pores. EPMA analyses indicate that halos are mixtures of forsterite and anorthite. Figure 1g shows an AOA that contains a large Ca-Al-rich nodule. Alternatively, it may be classified as a Ca-Al-rich inclusion with a thick forsterite rim. The Ca-Al-rich part consists of diopside, melilite and spinel.

Figure 2 shows trajectories of minor element concentrations during equilibrium condensation of olivine (olivine is equilibrated with Ca-Al-rich condensates and the gas phase) in a nebula at a total pressure of 10^{-4} bar with a dust enrichment factor of 1 (nominal solar composition). Under these conditions, condensation of olivine starts at ~1370 K. At this temperature, olivine is Ca-rich (CaO ~ 0.8 wt%). As temperature falls, it becomes progressively depleted in Ca and enriched in more volatile elements such as Cr, Mn, and Fe. The maximum olivine abundance is reached at ~1300 K; at lower temperatures olivine is partly consumed by reaction with the ambient gas to form pyroxene. While the MnO and FeO concentrations in olivine steadily increase with falling temperature, the CrO concentration depends on the presence or lack of a Cr-rich spinel in the condensation sequence. When a Cr-rich spinel becomes stable below ~1200 K, it scavenges Cr out of olivine. As a result, an initial increase of the CrO concentration in olivine at high temperatures (>1200 K) would be followed by a rather rapid drop at temperatures below 1200 K. Because chromite was not observed in the AOAs, in the current run the condensation of Cr-rich spinel was suppressed. Therefore, CrO in olivine (Fig. 2) continues increasing with decreasing temperatures. The MnO trajectory is generally similar to that of CrO, but the increase in MnO occurs at a lower temperature and is steeper than that of CrO. The relationships between MnO and CaO, and between CrO and CaO depend on the dust enrichment factor. A slight dust enrichment with a factor of ~2 apparently does not cause significant differences, but at an enrichment factor of 5 or higher, equilibrium MnO and CrO concentrations are higher compared to those shown in Fig. 2. For instance, a steep increase in MnO starts at CaO ~ 0.2 wt% for 5× dust enrichment, compared to that at CaO ~ 0.1 wt% for the nominal solar composition (Fig. 2).

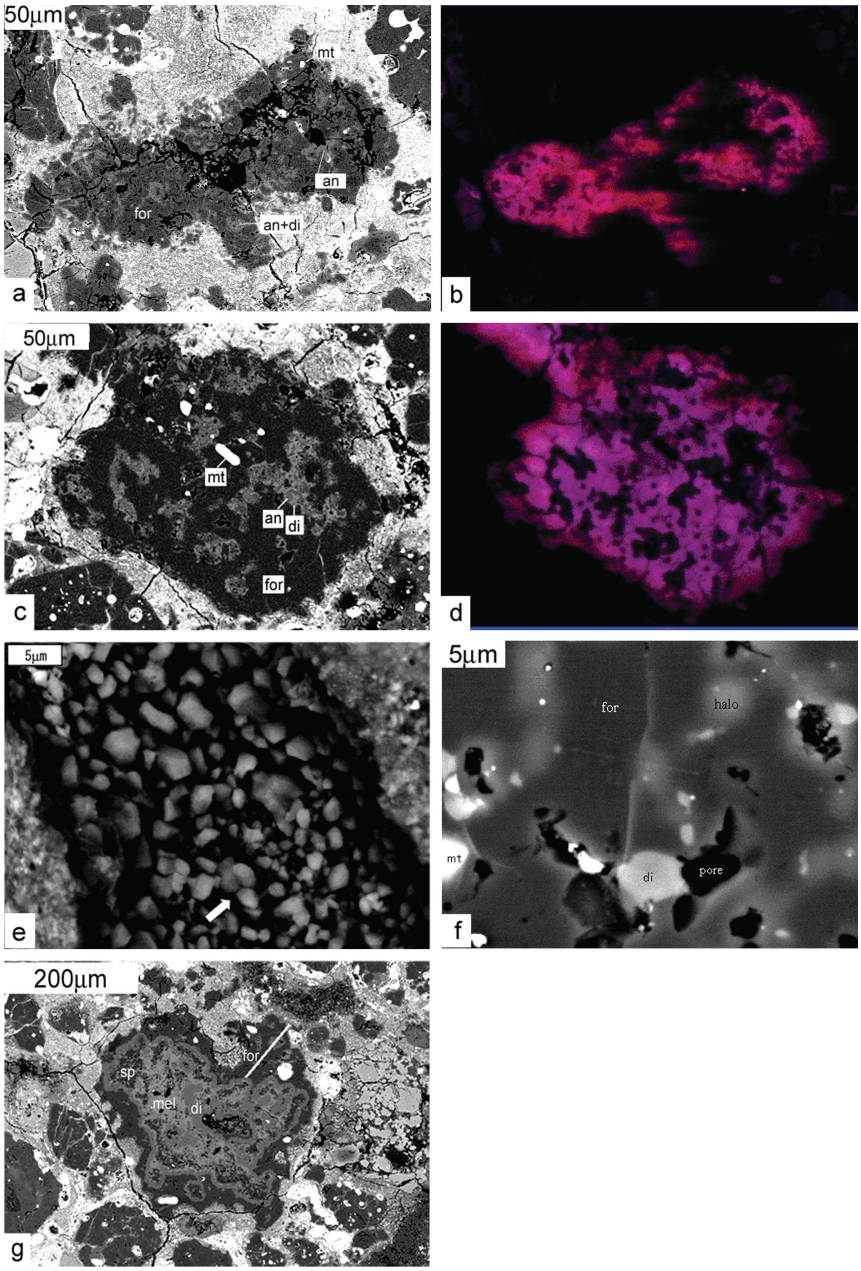

Fig. 1. a) Backscattered electron image of a porous AOA (AOA-A) in Y-81020. In addition to forsterite (for), it contains aluminous diopside (di), anorthite (an), and a few metal (mt) grains. Grain sizes of olivine and Ca-Al-rich materials appear relatively small. Numerous small pores seem to be indigenous, while large pores were probably produced during section preparation. Such large pores are more often observed in porous AOAs than in compact AOAs, suggesting the more fragile nature of porous AOAs. The shapes of porous AOAs tend to be more irregular than compact AOAs. b) CL image of the porous AOA (AOA-A) in Yamato 81020 at the same magnification. In general, the CL color of porous AOAs is more reddish than that of compact AOAs. c) Backscattered electron image of a compact AOA (AOA-B) in Y-81020. In addition to forsterite (for), it contains aluminous diopside (di), anorthite (an), Fe-Ni metal (mt), and small spinel (not seen at this magnification) grains. Grain sizes of olivine and Ca-Al-rich materials appear larger than those in porous AOAs. The core regions show pinkish CL whereas the rim regions (<10 µm from the boundary with matrix) show dark reddish CL. This AOA is certainly polycrystalline, but Mn (and Cr) did not diffuse through the grain boundaries. The entire AOA acted as if it were a single crystal with respect to Mn (and Cr) diffusion. d) CL image of the compact AOA (AOA-B) in Y-81020 at the same magnification. Small (a few µm) dark spots are the probe spots. e) Backscattered electron image of a porous fine-grained AOA in Murchison. A few triple junctions are seen in the lower central area. One of them is indicated by an arrow. Dark area around olivine grains is void space that was presumably produced during the sample preparation. f) Backscattered electron image of the interior portion of an AOA in ALH 77307. It consists of forsteritic olivine (for), diopside (di), metal (mt), diffuse area (halo), and pores. The halos are a mixture of anorthite and forsterite. g) Backscattered electron image of AOA-D in Y-81020 containing a large Ca-Al-rich nodule. The white line shows the location of the EMPA traverse across a forsterites (for) layer. The minor element data are shown in Figs. 3 and 4. The Ca-Al-rich nodule consists of diopside (di), melilite (mel), and spinel (sp).

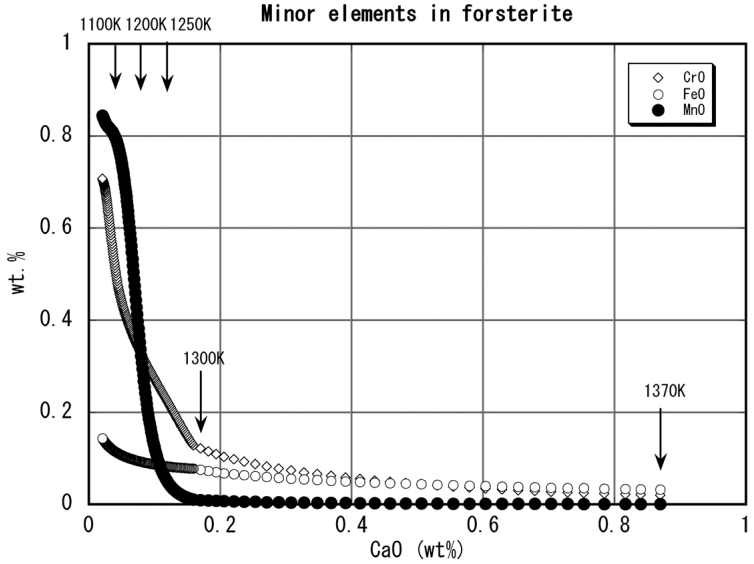

Fig. 2. Trajectories of minor element concentrations in forsterite during its condensation in a cooling nebula with solar elemental composition. The initial olivine condensate is rich in Ca and poor in more volatile elements (Fe, Mn, and Cr). As temperature falls, volatile element concentrations increase. The calculation was stopped at 1000 K where almost all volatile elements have condensed.

The trajectories shown in Fig. 2 are terminated at 1000 K where most of volatile elements have condensed. It is noted that although the MnO in olivine at this temperature is fairly high, it is not as high as that observed in some olivine grains in primitive meteorites and interplanetary dust particles (Klock et al. 1989).

The MnO, CrO, and CaO compositional data are shown in Figs. 3–6 and typical olivine compositions are given in Table 1. Some of the olivine data showed correlated high Ca and Al concentrations. These are presumably due to the presence of tiny Ca-Al-rich grains in AOAs and were omitted from the reported data. Some of the data which showed correlated high Fe and Ni concentrations were also omitted because they were presumably affected by metal grains in AOAs. Also, some data with poor totals and/or olivine stoichiometry were omitted. The criteria for omission were the following; Al_2O_3 > 0.24 wt%, CaO > 1.17 wt%, NiO > 0.13 wt%, total oxide <97.64 wt% (This condition was not applied to the Y-81020 AOA-A and AOA-B data because the average value of the total was 97.5% for the whole data set.), Si <0.98 per 4 oxygen formula unit.

Weisberg et al. (2004) reported that volatile elements (Cr and Mn) are enriched at the edges of AOAs. To test for possible radial zoning of AOAs from Y-81020, we measured minor element concentrations from the CL-red edges (within 10 micrometers from the olivine-matrix interface) and the CL-pinkish cores (more than 10 micrometers from the interface) of these AOAs. In porous AOAs from Acfer 094 the distinction between such cores and edges is difficult and was not made. AOAs in Acfer 094 have been previously described by Krot et al. (2004b).

The olivine compositions of this study are consistent with the compositions previously reported for AOAs in Acfer 094 (Krot et al. 2004c) and those for AOAs in Y-81020 (Chizmadia et al. 2002). We note that Fe contents in olivine are generally low. Similarly low FeO concentrations in AOA olivine from CR chondrites were reported by Weisberg et al. (2004). Some of the olivine (mostly from porous AOAs), however, shows FeO concentrations higher than ~0.7 wt%. This is much higher than those predicted by equilibrium condensation calculations (Fig. 2). We are not sure if such high FeO reflects nebular processes or contributions from matrix materials. Since the high FeO is mostly observed in porous AOAs, the latter possibility cannot be excluded. For this reason, FeO data are not discussed in detail in this study. Because of the low Cr and Mn concentrations in the matrices, possible contamination of MnO and CrO in olivine by matrix materials is negligible.

The MnO versus CaO and CrO versus CaO diagrams for 4 AOAs from Y-81020 are shown in Figs. 3 and 4, respectively. Cr is assumed to be divalent to be consistent with the thermodynamic calculations shown in Fig. 2. The MnO, CrO, and CaO data from the cores and edges of three AOAs are shown by solid and open symbols, respectively. Among 4 AOAs, one (AOA-A, Fig. 1a) is porous whereas three others are compact. The porous AOA-A is enriched in Mn and Cr and depleted in Ca, in contrast to the more refractory nature of compact AOAs. Enrichments of Mn and Cr at edges are well recognized by comparing the core data (solid symbols) and edge data (open symbols) for compact AOAs (AOA-B and AOA-C). The enrichments in Mn and Cr in the edges (Figs. 3 and 4) and their correlations with Ca suggest that equilibrium was not maintained during olivine condensation.

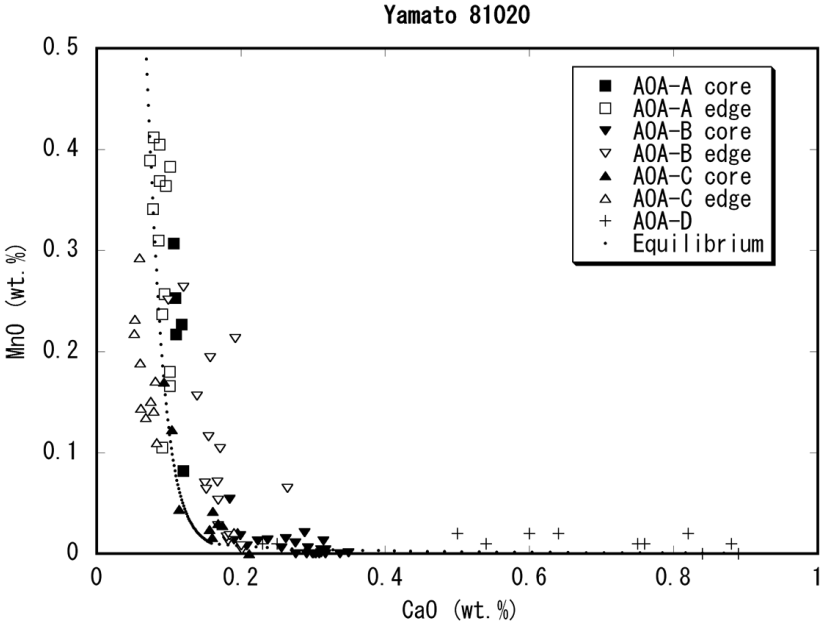

Fig. 3. MnO versus CaO diagram for 4 AOAs from Y-81020. Data from the core region are shown by solid symbols whereas those from the edge regions are shown by open symbols. Data for AOA-D are taken along the line shown in Fig. 1g. Small solid circles show the equilibrium trajectory for forsterite.

AOA-D (Fig. 1g) is very well sintered and has exceptionally high CaO concentrations up to >0.8 wt%. It shows a CaO concentration gradient across the forsterite layer that surrounds Ca-Al-rich materials. The MnO versus CaO and CrO versus CaO data of AOA-D shown in Figs. 3 and 4 were measured along the traverse shown in Fig. 1g. The Ca concentrations are high closest to the Ca-Al-rich materials. Ca X-ray contributions from the adjacent Ca-Al-rich nodules as a contributor to the high Ca concentrations can be ruled out because Al concentrations are low. Gradients in Ca concentrations are not pronounced in other AOAs, but there is a tendency for Mn and Cr to be enriched in the edges whereas Ca is enriched in the cores of AOAs (Figs. 3 and 4). This is consistent with the observations by Weisberg et al. (2004).

The MnO versus CaO and CrO versus CaO diagrams for Acfer 094 are shown in Figs. 5 and 6, respectively. Figure 5 is similar to Fig. 3 and Fig. 6 is similar to Fig. 4. However, a closer look reveals that Ca-poor compositions are more abundant in Acfer 094. The difference between Y-81020 and Acfer 094 is mainly attributable to a larger number of porous AOAs in Acfer 094 compared to Y-81020.

Figures 3 and 5 apparently show a good agreement between the equilibrium trajectory and AOA data for MnO versus CaO. Similarly good agreement is seen for CrO versus CaO (Figs. 4 and 6). But equilibrium was not maintained for minor elements (Mn, Cr, and Ca) in forsterite (Figs. 3 and 4). The trends between MnO and CaO (Figs. 3 and 5) and between CrO and CaO (Figs. 4 and 6) are qualitatively explained as due to anti-correlations between refractory Ca and more volatile Mn and Cr.

DISCUSSION

Parent-Body Alteration

Effects of parent-body alteration on AOAs in CO3 chondrites were studied by Chizmadia et al. (2002). They showed that minor elements in AOA olivine in CO3.0 were not affected by parent body alteration, whereas at types higher than 3.2, Fe enters olivine by diffusion. All chondrites studied here are as primitive as CO3.00–CO3.05 (Kimura et al. 2008) and show no systematic enrichment in Fe. While all olivine grains in the CO chondrites of petrologic types higher than 3.2 show FeO enrichment at edges, only a limited number of forsterite analyses in Acfer 094 and Y-81020 have FeO concentrations (>0.7 wt%) indicative of contamination of these analyses rather than of a metamorphic effect. A detailed petrologic study (Krot et al. 2004b) of Acfer 094 (ungrouped carbonaceous chondrite) showed that aqueous alteration is insignificant in this chondrite. Aqueous alteration is more pervasive in Murchison (CM2). But AOA forsterite seems to be fairly resistant to this type of alteration (Krot et al. 2005). Therefore, minor elements in the forsterite are considered to have been not affected by metamorphism or aqueous alteration, but reflect nebular processes.

Ca-Poor Forsterite

A salient feature of AOA forsterite is its depletion in CaO. Figures 3–6 show that most AOA forsterites contain <0.3 wt% CaO. Similar data for Acfer 094 AOAs have been reported by

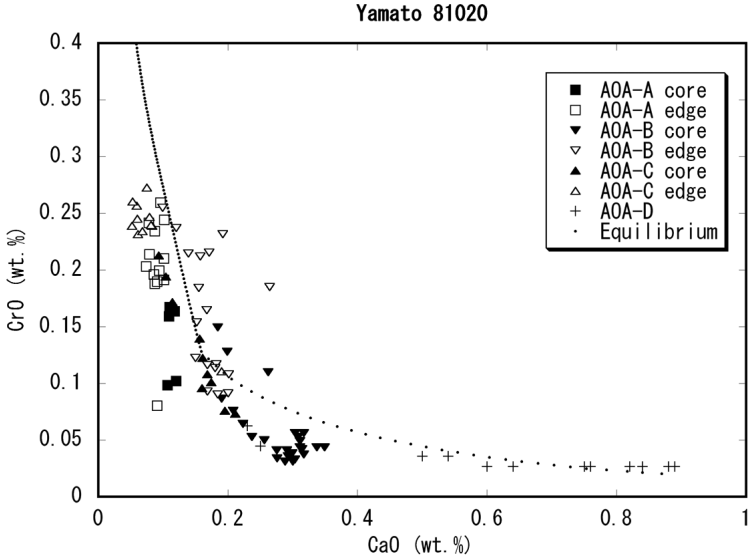

Fig. 4. CrO versus CaO diagram for 4 AOAs in Y-81020. Data from the core region are shown by solid symbols whereas those from the edge regions are shown by open symbols. Data for AOA-D are taken along the line shown in Fig. 1g. Small solid circles show the equilibrium trajectory for forsterite.

Krot et al. (2004c). In contrast, refractory forsterites mostly contain more than ~0.4 wt% CaO (e.g. Pack et al. 2004). High CaO concentrations in refractory forsterite are well explained by equilibration with high-CaO silicate melt at high temperatures (Pack and Palme 2003). The AOA-D from Y-81020 with high CaO concentrations in olivine (Figs. 3 and 4), though exceptional among the present data set, proves that high CaO concentrations should be observed if equilibrium at high temperatures was maintained. It is the depletion in CaO in many AOA forsterites that needs to be explained.

Difficulty in Maintaining Equilibrium Concentrations of Ca Down to ~1100 K in Olivine Larger than 1 μm in Radius

There are difficulties in explaining the AOA data by equilibrium condensation during slow cooling. The main difficulty is the low Ca concentrations in olivine. According to the simulation of equilibrium condensation (Fig. 2), initial olivine condensate contains ~0.87 wt% of CaO. Essentially all olivine is condensed at ~1300 K, where CaO concentration is ~0.16 wt%. Nevertheless, CaO concentrations in AOA olivine are as low as ~0.05 wt%. Therefore, olivine, if produced by an equilibrium process, must lose Ca during cooling. (The decrease in CaO from 1370 K to 1300 K may be considered as dilution of initially high CaO with a large amount of forsterite condensate. At lower temperatures, Ca has to be either evaporated or transported to other minerals by diffusion.) To evaluate if this is possible we use the concept of a closure temperature.

A closure temperature (T_c) depends upon diffusion rate (D_0 exp(-E/RT) where D_0 is the pre-exponential factor, E is the activation energy, R is the gas constant and T is the absolute temperature), a characteristic grain size (a) and a characteristic cooling time (τ) which is inversely proportional to the cooling rate. It is expressed as $T_c = R/[E\ ln(A\tau\ D_0/a^2)]$ (Dodson 1973). Here, A is a numerical constant dependent on geometry. Unless specified otherwise, spherical geometry is used in the following discussion. Diffusion rates of Ca, Cr, and Mn in olivine are summarized in Fig. 7. Ca diffusion should be slow because of its large ionic radius. Heating experiments of olivine performed by Jones and Lofgren (1993) suggested that Ca diffusion rates at 1450–1500 K are much slower than those of Mn and Fe, consistent with the expectations. It is known that Fe-bearing and Fe-free olivine show systematically different activation energies for diffusion (Fig. 7). There are two systematic studies on Ca diffusion rates in forsterite (Morioka 1981; Hain 1998). The former was performed in air whereas the latter was measured at an fO_2 of 10^{-10} bars. Combining these two data sets, Coogan et al. (2005) reported diffusion rates for forsterites at an fO_2 of 10^{-10} bars. Since the oxygen fugacity dependence is quite weak we adopted the value at an fO_2 of 10^{-10} bars ($D_0 = 2.5$ cm^2/s and E = 403 kJ/mol) for calculations of Ca closure temperatures.

Mn diffusion in forsterite ($D_0 = 9690$ cm^2/s, E = 429 kJ/mol) (Morioka 1981) is faster than Ca diffusion. Cr diffusion in pure forsterite has not been studied yet. Therefore, we used Cr diffusion rates ($D_0 = 0.0022$ cm^2/s, E = 299 kJ/mol) in Fe-bearing olivine (Ito and Ganguly 2006) for calculations of Cr closure temperatures. However, the activation energy for Cr is considerably smaller than those for Ca or Mn presumably because of the presence of Fe in the olivine. Hence Cr diffusion rates in forsterite may be significantly different from those shown in Fig. 7. Because

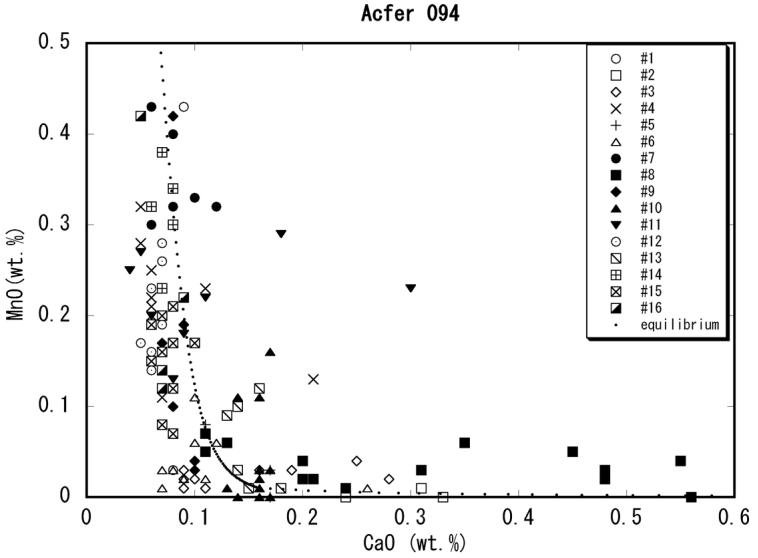

Fig. 5. MnO versus CaO diagram for the Acfer 094 AOAs. Sixteen AOAs are shown by different symbols. Small solid circles show the equilibrium trajectory for forsterite.

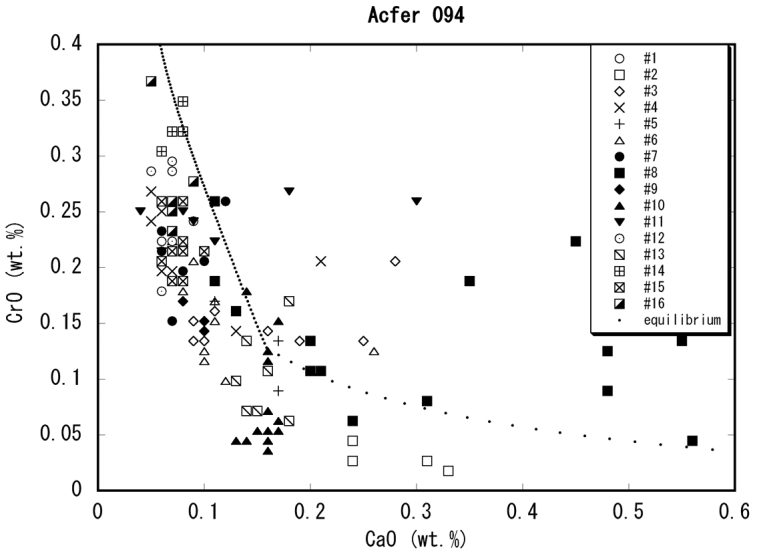

Fig. 6. CrO versus CaO diagram for the Acfer 094 AOAs. Sixteen AOAs are shown by different symbols. Small solid circles show the equilibrium trajectory for forsterite.

of this uncertainty in the choice of diffusion rates of Cr and because both Mn and Cr play similar roles as volatile elements in contrast to refractory Ca, in the following discussion we mainly concentrate on Mn.

In calculations of closure temperatures olivine grain sizes are assumed to range from 1 μm (typical size observed in the fine-grained AOA from Murchison, Fig. 1e) to 10 μm (typical size observed in many AOAs).

There are many ways of estimating the cooling rates of AOAs. Theoretical studies predict slow cooling at ~0.002 K/h for the whole nebula at 1 AU through ~1000 K (e.g., Watanabe et al. 1990). Typical cooling rates of coarse-grained type B CAIs range from 0.5 to 50°K/h (Stolper 1982; MacPherson et al. 1984; Beckett et al. 1990; Davis et al. 1992). A fine-grained mixture of spinel and diopside replacing melilite is often observed in Ca-Al-rich materials in AOAs (Krot et al. 2004c). Such fine-grained materials are indicative of rather rapid cooling. Quantitative estimates of cooling rates based on such features have not been done, but they are probably similar to those of type B CAIs. Such a quick cooling might have been associated with reconnection of the solar magnetic field lines (Feigelson et al. 2006).

The grain size of forsterite is a function of the cooling rate if the condensation occurred by homogeneous nucleation.

Table 1. Representative olivine compositions (wt%) in AOAs from Y-81020 and Acfer 094.

	Y-81020 AOA-A edge	Y-81020 AOA-B edge	Y-81020 AOA-B core	Y-81020 AOA-C edge	Y-81020 AOA-C core	Y-81020 AOA-D
CL color	Red CL	Red CL	Pink CL	Red CL	Pink CL	Pink CL
MgO	53.91	54.79	54.86	55.31	55.51	56.44
Al_2O_3	0.03	0.03	0.05	0.02	0.03	0.03
SiO_2	41.67	42.22	42.14	42.32	42.65	42.28
CaO	0.09	0.10	0.30	0.06	0.21	0.76
TiO_2	<0.02	<0.02	0.04	0.02	0.03	<0.02
V_2O_3	<0.02	0.03	0.04	<0.02	0.02	<0.02
CrO	0.20	0.26	0.03	0.26	0.07	0.03
MnO	0.31	0.25	<0.03	0.29	<0.03	<0.03
FeO	0.92	0.68	0.27	0.66	0.31	0.32
NiO	<0.05	0.05	<0.05	<0.05	<0.05	<0.05
Total	97.22	98.42	97.76	98.98	98.84	99.89

	Acfer 094 AOA-1	Acfer 094 AOA-2	Acfer 094 AOA-3	Acfer 094 AOA-4	Acfer 094 AOA-5	Acfer 094 AOA-6
CL color	Red CL	Pink CL	NA	NA	NA	red CL
MgO	55.71	56.33	56.60	57.01	56.65	56.34
Al_2O_3	0.02	0.05	0.08	<0.02	0.03	<0.02
SiO_2	41.77	41.28	42.35	42.73	52.39	42.27
CaO	0.09	0.24	0.11	0.07	0.13	0.10
TiO_2	0.03	0.04	0.04	0.02	0.03	0.03
V_2O_3	0.02	0.02	0.03	0.02	0.02	<0.02
CrO	0.24	<0.03	0.16	0.20	0.16	0.13
MnO	0.43	<0.03	<0.03	0.16	0.06	0.11
FeO	0.69	0.53	0.46	0.50	0.39	0.29
NiO	<0.05	<0.05	<0.05	<0.05	<0.05	<0.05
Total	99.02	98.57	99.84	100.75	99.89	99.31

	Acfer 094 AOA-7	Acfer 094 AOA-8	Acfer 094 AOA-9	Acfer 094 AOA-10	Acfer 094 AOA-11	Acfer 094 AOA-12
CL color	NA	NA	NA	NA	NA	NA
MgO	55.76	56.38	55.92	56.35	54.23	55.86
Al_2O_3	0.02	0.03	0.07	0.02	0.04	0.05
SiO_2	41.99	41.62	41.33	41.76	42.50	41.76
CaO	0.08	0.20	0.09	0.15	0.30	0.06
TiO_2	<0.02	0.03	0.02	0.03	0.05	0.03
V_2O_3	0.02	0.03	0.03	0.02	<0.02	0.03
CrO	0.20	0.11	0.28	0.05	0.26	0.21
MnO	0.32	<0.03	0.19	<0.03	0.23	0.14
FeO	0.52	0.50	0.74	0.41	0.72	0.59
NiO	<0.05	<0.05	<0.05	<0.05	<0.05	<0.05
Total	98.93	98.94	98.67	98.83	98.38	98.76

	Acfer 094 AOA-13	Acfer 094 AOA-14	Acfer 094 AOA-15	Acfer 094 AOA-16
CL color	NA	NA	NA	NA
MgO	56.72	55.48	56.18	56.01
Al_2O_3	0.02	<0.02	0.02	0.03
SiO_2	42.29	40.85	42.08	41.76
CaO	0.15	0.07	0.08	0.07
TiO_2	0.02	<0.02	0.02	0.03
V_2O_3	0.02	0.02	0.03	0.02
CrO	0.07	0.32	0.21	0.25
MnO	<0.03	0.38	0.12	0.12
FeO	0.68	0.72	0.58	0.49
NiO	<0.05	<0.05	<0.05	<0.05
Total	100.01	97.87	99.34	98.80

NA: not available.

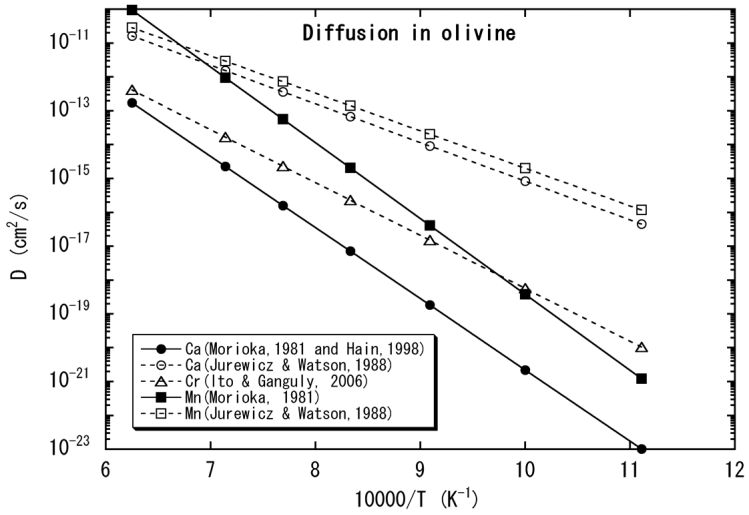

Fig. 7. Diffusion rates of Ca, Cr, and Mn in olivine. Mn and Ca diffusion rates in forsterite are shown by solid symbols and solid lines. Diffusion rates in Fe-bearing olivine are shown for comparison by open symbols and dashed lines. The difference in the activation energies between the Fe-free and Fe-bearing olivines is clearly seen. The Cr diffusion rate of Ito and Ganguly (2006) obtained from Fe-bearing olivine was used for Cr closure temperature calculations, but may not be applicable to the AOA forsterite.

Although the surface energy of forsterite which is necessary for the estimate of grain size by homogeneous nucleation is not well known, for a grain of 1 μm in size at a nebular pressure of ~10^{-4} bar a cooling rate of ~0.002 K/s (7.2 K/h) is estimated based on the diagrams of Imae et al. (1993). This estimate is based solely on theoretical considerations (Kozasa and Hasegawa 1987) and may have large uncertainties. In addition, it is also not clear whether condensation occurred by homogeneous nucleation.

The absence of pyroxene on most AOA forsterites (Krot et al. 2004a) also provides evidence for a rapid cooling because pyroxene should have formed if AOAs cooled slowly (Imae et al. 1993). According to Imae et al. (1993), a pyroxene layer ~0.1 μm thick should form at a cooling rate of ~5×10^{-6} K/s (~0.02 K/h) at a nebular pressure of 10^{-4} bar. Because such pyroxene layers are not observed (at the detection limit of SEM) on most AOA forsterites, a cooling rate of >0.02 K/h is suggested.

Quantitative estimates of cooling rates can also be made based on the core-edge structure of compact AOAs observed by CL, assuming that the structure was produced by an inward diffusion of Mn during the last cooling episode. The core-edge structure reflects Mn (and Cr) diffusion from the AOA surface. For a rim grain of 10 μm (r = 5 μm) at the cooling rate of 5×10^{-7} K/s (~0.002 K/h), the Mn closure temperature is ~1164 K for one-dimensional diffusion. At this temperature olivine is expected to contain high (~0.49 wt%) MnO. At the cooling rate of ~5×10^{-5} K/s (~0.2 K/h) the Mn closure temperature is ~1292 K for one-dimensional diffusion. At this temperature olivine is expected to contain very low (~0.015 wt%) MnO. (Here we should note that these evaluations based on closure temperatures given by $T_c = R/[E\ ln(A\tau\ D_0/a^2)]$ are not very accurate, because the equilibrium MnO concentration at the grain surface, which should be constant if we apply the original formula for T_c, is not constant. In order to examine such an effect, we conducted more refined numerical simulations of Mn diffusion in olivine by taking into account the change in MnO concentration at the grain surface during temperature drops. Such refined calculations, however, gave similar results with those obtained above, justifying the evaluations based on closure temperatures.) Thus, the cooling rate of 0.002 K/h is broadly consistent with the Mn profile at the rim, whereas the cooling rate of ~0.2 K/h is too fast. However, if there were multiple reheating episodes after the AOAs aggregation, then Mn could diffuse inward from the surface during reheating as long as the temperature is not high enough for nearly complete Mn evaporation. Therefore, the CL core-rim structure puts a lower limit on the cooling rate.

Table 2. Closure temperatures of spherical olivine grains.

	dT/dt = -5×10^{-6} K/s		dT/dt = -5×10^{-5} K/s	
	r = 1 μm	r = 10 μm	r = 1 μm	r = 10 μm
Ca	1242 K	1399 K*	1316 K	1493 K*
Cr	1121 K	1296 K	1203 K	1404 K*
Mn	1099 K	1212 K	1153 K	1278 K

*Closure temperatures higher than the initial temperature (1370 K) mean that a grain is already a closed system when it grows to that size.

Since many AOAs experienced reheating episodes, the cooling rates estimated based on the AOA petrology are not necessarily those of forsterite condensation. In summary, we think that the most reliable estimate of the cooling rate during condensation of AOAs is derived from the absence of pyroxene: >5×10^{-6} K/s (~0.02 K/h) at nebular pressure of 10^{-4} bar. The closure temperatures listed in Table 2 were calculated at this cooling rate. To illustrate how cooling rates

affect closure temperatures, they were also calculated at a faster cooling rate of 5×10^{-5} K/s.

The closure temperature of Ca in an olivine grain of 1 μm in radius at the cooling rate of 5×10^{-6} K/s is 1242 K. At this temperature such olivine grains equilibrated with ambient nebular gas and Ca-rich minerals should contain no less than 0.11 wt% CaO. The Cr and Mn closure temperatures at the same grain size and cooling rate are 1121 and 1099 K, respectively (Table 2). Although the equilibrium CrO concentration of 0.43 wt% is broadly consistent with the AOA data (Figs. 4 and 6) the predicted MnO concentration of ~0.8 wt% is too high compared to the observed values (Figs. 3 and 5). An olivine grain of 10 μm in radius cooling at the same rate of 5×10^{-6} K/s has Ca, Cr, and Mn closure temperatures of 1399, 1296, and 1212 K, respectively (Table 2). The chemical composition of such a grain (0.87 wt% CaO, 0.14 wt% CrO, and 0.17 wt% MnO—Fig. 2) is clearly inconsistent with both the equilibrium calculations and the observed data. Thus, equilibrium condensation even at slow cooling rates is not a viable explanation for the low CaO concentrations in AOA olivines, if the initial grain size was not much smaller than 1 μm.

Disequilibrium Condensation with Respect to Ca

A plausible explanation for the low CaO concentrations in AOA olivines is a disequilibrium condensation with respect to Ca. In the temperature range of AOA olivine condensation (1300 K ~ 1370 K), almost all Ca is locked up in Ca-Al-rich materials, with only a small fraction (0.00016) remaining in the gaseous phase. Therefore, if olivine grains were instantaneously made from gaseous Mg, SiO, Ca, and H_2O molecules, then the Ca concentration in olivine would be very small (a few ppm). To achieve equilibrium Ca concentration in forsterite, a lot of Ca has to be transported either by solid state diffusion from adjacent Ca-rich solid materials or by vapor phase transport from Ca-rich condensates which may exist in the vicinity. But such transport is not efficient because of both the very slow diffusion rate of Ca in solid materials and the very low Ca vapor pressure. Thus, the low Ca concentrations in AOA olivines are well explained by disequilibrium condensation.

There remains a problem of explaining the correlated variations among MnO (CrO), CaO and texture of AOAs (porous or compact). One way of explaining the correlated variations is reheating. During reheating, Mn is lost by evaporation, Ca is acquired by diffusion from adjacent Ca-rich minerals and AOAs become compact by sintering. Alternatively, compact AOAs might have formed during slow cooling. In such a case, the CaO variations in AOA forsterites correlated with the AOA texture are caused by variations in Ca vapor pressure which is controlled by cooling rates through evaporation kinetics. These scenarios are quantitatively examined below.

Formation of Compact AOAs by Reheating

As mentioned above, CaO concentrations in olivine are likely to depend on the kinetics of Ca vapor replenishment during olivine condensation which occurs at a temperature not much below the equilibrium condensation temperature. The fine-grained aggregate (Fig. 1e) in Murchison suggests a rapid cooling during condensation, which tends to limit the replenishment of sufficient Ca vapor. The exact degree of Ca deficiency is hard to predict. Here we simply assume that the CaO concentration in olivine condensates was ~0.05 wt%, which is the lowest value observed in AOAs. We chose this value because the higher CaO values observed in compact AOAs can result from reheating events. In contrast, an assumption of higher initial CaO concentrations in olivine will make later removal of CaO impossible because of the high Ca closure temperature.

Based on these considerations, we assume that small (1 μm) olivine grains with low CaO (~0.05 wt%) and rather high MnO (0.4 wt% MnO) and CrO (0.3 wt% CrO) (Figs. 3–6) condensed during cooling from 1370 to ~1100 K and then aggregated to form proto-AOAs. We assume that all AOAs were initially fine-grained and porous, with the minor element concentrations being similar to the above values. Petrographic observations show that most AOAs have experienced reheating after the aggregation (Aléon et al. 2002; Krot et al. 2004a). Therefore, variable minor element concentrations in AOAs are likely to have been established during reheating events.

There are only a few studies on sintering of olivine (e.g., McDonnell et al. 2002). The experiments were not performed on loose aggregates like AOAs and the sintering effects were not presented quantitatively. Therefore, the applicability of this study to AOAs needs to be examined by further studies. Also, because the numbers used in the following discussion were read from the figures, these are somewhat uncertain. McDonnell et al. (2002) showed that heating at 1673 K for 1 h reduces the porosity of an olivine aggregate from ~50% to 8%. Assuming that sintering is controlled by oxygen diffusion (Ryerson et al. 1989), a similar degree of sintering is achieved in 6.8×10^5 s, 8.1×10^6 s and 1.4×10^8 s at 1400, 1300, and 1200 K, respectively. These time scales are not exceedingly long for heating in the solar nebula at temperatures higher than 1200 K.

Because the compact AOAs tend to contain less Mn and Cr than the porous AOAs (compare compact AOA-B, C and D with porous AOA-A in Figs. 3 and 4 and also compare generally more compact Y-81020 AOAs [Figs. 3 and 4] with more porous Acfer 094 AOAs [Figs.5 and 6]), the reheating temperature must be high enough (>1300 K) for the equilibrium Mn and Cr concentrations to be low. For example, at 1300 K well-sintered AOAs may be formed in ~8.1×10^6 s. Most of the time, the reheating temperature must be lower than ~1370 K to prevent olivine evaporation, although it might have exceeded 1370 K briefly. Thus, the reheating temperatures are in the range of 1300 ~ 1370 K. This is

below the solidus temperature of Ca-Al-rich materials in the AOAs (Stolper 1982), consistent with the lack of extensive melting of Ca-Al-rich materials. Almost all Mn and a large fraction of Cr will be lost by volatilization during reheating. At 1300 K the diffusion length for Mn is 13 μm per year. Therefore, even if the grains grew somewhat during the reheating, Mn can be lost in one year or so during reheating. CaO concentrations in olivine may increase by diffusion from adjacent tiny diopside grains. However, because Ca diffusion is slow its diffusion lengths are 0.7 μm and 1.8 μm per year at 1300 K and 1370 K, respectively. Hence, it is not easy to explain the CaO concentrations in the core of compact AOAs (e.g. 0.20~0.35 wt% CaO in AOA-B) by reheating. If an AOA were heated at 1300 K for 100 years, CaO concentrations in forsterites that are located more than 10 μm away from Ca-Al-rich nodules are little changed from the initial value (0.05 wt%). If an AOA were heated at 1370 K for 100 years, then Ca would diffuse ~18 μm from Ca-Al-rich nodules showing pronounced CaO concentration gradients which are not observed. High Ca halos (Fig. 1f) that appear to consist of a mixture of olivine and anorthite were observed in an AOA from ALH 77307. We interpret this feature as a result of a brief very high temperature (T > 1370 K) reheating. If such halos were subsequently heated at 1300 ~ 1370 K for a long time, then the high CaO concentrations in core olivine may be achieved. However, we emphasize that in order to explain high CaO concentrations in core olivine in compact AOAs a time scale of more than 1 year is needed.

In the rare case of AOA-D in Y-81020 (Fig. 1g), high Ca concentrations are observed in olivine located tens of micrometers away from Ca-Al-rich nodules. It takes hundreds of years for Ca to diffuse over such a distance at 1370 K. If such a long heating time is unrealistic, then it may be necessary to invoke formation of AOAs in a dust-enriched system that allows having higher reheating temperatures without significant olivine evaporation.

Pyroxene becomes stable below 1300 K in a nebula of solar composition. According to Imae et al. (1993), formation of ~1 μm thick pyroxene layer at 1300 K will take ~10^8 s, much longer than the time required for sintering (~8.1×10^6 s at 1300 K). Therefore, pyroxene is unlikely to be produced during sintering.

As discussed earlier, the CL core-edge structure of compact AOAs provides an estimate of the cooling rate during the last cooling episode. In terms of isothermal heating, diffusion of Mn for ~10 μm at 1200 K (when most Mn is condensed) takes about 16 yr. Such a time scale is not inconsistent with the above-estimated reheating time scales based on sintering kinetics and/or the lack of pyroxene in AOAs. This estimate is also consistent with the estimated reheating time scale from partial resetting of oxygen isotopic compositions in AOAs (Fagan et al. 2004). Although the majority of AOAs seems to show the CL core-edge structure, some AOAs do not. In such AOAs, Cr and Mn are depleted right at the edge as expected from CL images. These AOAs might have been removed from the AOA formation regions before the temperature drops below the condensation temperatures of Mn and Cr. The whole process that produced AOAs including the initial condensation, aggregation, sintering, and final cooling was completed in a short time compared with the half-life of ^{26}Al, as suggested by the recently measured canonical initial ratio of ^{26}Al/^{27}Al (Itoh et al. 2007; Sugiura and Krot 2007).

Formation of Compact AOAs During Initial Slow Cooling

The discussion above assumed that the fine-grained, porous AOAs formed first as aggregates of nebular condensates while the compact AOAs formed later by reheating of the fine-grained, porous precursors. However, it may be possible to form well-sintered, compact AOAs during initial cooling if the cooling rate was slow enough. Despite the very low Ca vapor pressure in the ambient nebular gas (~10^{-13} bar), slow cooling may allow enough Ca to evaporate from Ca-rich solid phases, leading to higher, near-equilibrium CaO concentrations in the compact AOAs. At present, we do not have reliable estimates of CaO concentrations in condensed forsterites. Here we assume appropriate concentrations of CaO have condensed in forsterites and examine the accretion time scale of AOAs and then evaluate if sintering is possible during slow cooling.

The accretion time scale t_{acc} is expressed as $1/(n\sigma \Delta V_{rel})$ (Nakagawa et al. 1981). Here, n is the number density of olivine grains, σ is the collisional cross-section and ΔV_{rel} is the relative velocity between two grains. σ is calculated as $\pi(r_1 + r_2)^2$, where r_1 and r_2 are radii of two colliding grains. For a crude estimate of the number density n, we assume that all Mg in the nebula is locked up in olivine. Then, based on the forsterite stoichiometry, the amounts of silicon and oxygen incorporated into olivine are calculated. The total amount of olivine is calculated based on the solar abundance of Mg (Anders and Grevesse 1989). The number density of olivine grains with r = 1 μm is estimated to be n ~ 0.36/cm^3 at 1300 K and 10^{-4} bar. The relative grain velocity caused by the Brownian motion is estimated to be ~0.3 cm/s (Nakagawa et al. 1981). The relative velocity due to the turbulent motion is estimated to be on the order of ~10 cm/s (Weidenschilling 1984). Accretion time scales corresponding to these velocities are 7×10^7 s and 2×10^6 s, respectively. At 10^{-4} bar, the sedimentation velocity toward the equatorial plane is slower than the velocity of Brownian motion for a grain of r = 1 μm. However, once the size of an aggregate becomes significantly larger than the size of single grains, the aggregate sinks much faster than the small grains making the accretion process more efficient (Nakagawa et al. 1981). Photophoresis is also effective in moving grains irradiated by the sun (Krauss and Wurm 2005; Wurm and Krauss 2006). It is particularly effective for aggregates because the photophoresis drift velocity is inversely proportional to thermal conductivities. Therefore, once small aggregates are

formed they capture individual grains and grow quickly. Hence, typical accretion time scales are probably ~2×10^6 s rather than 7×10^7 s. For the sake of completeness we examine sintering of forsterite in 4 cases which arise from combinations of accretion time scales and cooling time scales (Table 3). For simplicity, we assume that the accretion process starts at 1300 K when olivine is fully condensed.

The degree of sintering of an olivine aggregate during cooling is evaluated from the integrated diffusion length of oxygen that is normalized to the oxygen diffusion length of an artificially sintered olivine aggregate (heated for 1 h at 1673 K—see section Formation of Compact AOAs by Reheating for details). The integration of diffusion length is made over 200 K interval starting from the accretion temperature T_a. (Diffusion rates at T_a – 200 K are more than 4 orders of magnitude smaller than those at T_a). In the case of fast accretion ($\tau = 2 \times 10^6$ s) and slow cooling ($dT/dt = -5 \times 10^{-6}$ K/s), the degree of sintering is ~33%. This is equivalent to heating for ~0.1 h at 1673 K. According to the time dependence of sintering reported by McDonnell et al. (2002), the initial porosity is reduced to 1/2 by such sintering. In the other cases of Table 3, sintering during cooling is practically negligible. The above evaluation was made assuming the grain radius of ~1 μm. If grains are larger, then the relative velocities ΔV_{rel} are also larger (Dominik et al. 2006), but the size dependence is not particularly strong. Since n is inversely proportional to the size, the accretion time $1/(n\sigma \Delta V_{rel})$ is not significantly affected by the grain size.

In summary, it seems possible to make well-sintered aggregates if the cooling rate was ~5×10^{-6} K/s or slower and accretion was quick. If the grain radii had grown to ~10 μm during the early stage of cooling, then olivine grains were already closed systems with respect to Ca (Table 2). Qualitatively, higher CaO in larger (well sintered) AOAs (and lower CaO in porous AOAs) is well understood by kinetics of Ca vapor replenishment during cooling, although quantitative evaluation cannot be made at present. Figure 1b shows that a compact AOA has an effective grain size of ~100 μm for Mn (and Cr) diffusion. The closure temperature of Mn for r ~ 100 μm is 1352 K where 0.002 wt % of MnO is expected. Little MnO in the interior of compact AOAs is consistent with the high Mn closure temperature.

Long-Duration, High Temperatures at the Inner Edge of the Solar Nebula

It appears that both reheating of fine-grained AOAs and slow cooling during condensation and accretion can potentially explain the formation of compact AOAs. One concern about these scenarios is that a very long duration of high temperatures is needed for forming compact AOAs. For instance, the cooling rate 5×10^{-6} K/s (~0.02 K/h) estimated for the latter scenario, is much slower than those inferred from coarse-grained CAIs (0.5~50 K/h). It is possible that the fast cooling experienced by CAIs (and by porous AOAs) is associated with reconnection of magnetic field lines (Feigelson et al. 2006) in a relatively cool (not irradiated by the sun) region of the nebula. The long-duration, high temperatures experienced by compact AOAs imply that they would have been located in a hot region that was directly irradiated by the Sun.

Table 3. Accretion temperatures (T_a = 1300- $dT/dt \times t_{acc}$) and degrees of sintering.

	Slow cooling ($dT/dt = -5 \times 10^{-6}$ K/s)	Fast cooling ($dT/dt = -5 \times 10^{-5}$ K/s)
Slow accretion ($t_{acc} = 7 \times 10^7$ s)	950 K, negligible sintering	Very low T, negligible sintering
Fast accretion ($t_{acc} = 2 \times 10^6$ s)	1290 K, 33%	1200 K, 2.7%

The inner edge of the forsterite condensation front in the nebula is always irradiated by the sun because small amounts of large Ca-Al rich objects that are expected to be located closer to the sun would not block solar radiation effectively. Small (~1 μm) forsterite grains will be quite abundant and could make the nebula opaque in a short distance (~3000 km). Therefore, only a small fraction of AOAs is directly irradiated by the Sun and cools slowly during a fading phase of the central star. Most AOAs that are not directly irradiated by the sun cool more rapidly (after magnetic reconnection events) producing fine-grained, porous AOAs. This is consistent with the observation that the porous AOAs are more abundant than compact AOAs and that the compact AOAs tend to contain large Ca-Al-rich nodules (e.g. Fig. 1g) suggesting that they were located closer to the Sun than the fine-grained, porous AOAs which do not contain large Ca-Al-rich nodules. It may also be worth noting that forsterite grains irradiated by the Sun could have larger relative velocities due to photophoresis. Hence, their accretion time scale will be short. Together with slow cooling, this leads to formation of compact AOAs. Forsterite grains in the opaque nebula interior have smaller relative velocities because photophoresis is not effective. Hence their accretion time is long. Together with fast cooling, this leads to formation of fine-grained, porous AOAs.

CONCLUSIONS

AOAs hold many important clues to the thermal history of the nebula in which they formed, including the olivine grain sizes, the absence of pyroxene in many AOAs, the minor element concentrations in olivine, the sintered textures of many AOAs, and the core-edge structure in CL images. With the aid of simulations of olivine condensation and estimations of closure temperatures based on diffusion rates, the thermal history of AOAs in the nebula was examined quantitatively.

An important observation is that CaO concentrations are low, particularly in porous aggregates. A plausible explanation of this is apparently the lack of equilibrium during condensation of Ca in olivine. Fine-grained, porous AOAs formed in a quickly cooling nebula. Compact AOAs

may have formed either by reheating of fine-grained, porous AOAs or in a slowly cooling nebula region which was irradiated by the Sun.

Some important issues relevant to AOA formation still remain unresolved. First, it is not clear whether condensation of olivine occurred by homogeneous nucleation and condensation or by heterogeneous condensation on a pre-existing substrate. Second, we need to understand the kinetics of Ca replenishment in the nebular gas in order to evaluate whether this mechanism is capable of explaining CaO concentrations in AOA's olivines. Alternatively, CaO may be transported to olivine from adjacent Ca-rich phases by solid-state diffusion. Third, it is important to determine the nature (energy source, peak temperature, duration, and frequency) of the reheating events that seem to have affected many AOAs.

Acknowledgments–This work was supported by grant-in-aid of science research (14340169 for N. S., 16540435 and 19540500 for M. K.) from the Japanese Society for the Promotion of Science and NASA grants NNGO5GI66G and NNX08AH79G. The Acfer 094 polished sections were made available by Dr. A. N. Krot. We thank Dr. M. Ito for discussion on Cr diffusion rates in olivine grains. We thank Dr. M. K. Weisberg, Dr. A. Ruzicka, Dr. C. Floss, and an anonymous reviewer for valuable comments and suggestions.

Editorial Handling—Dr. Christine Floss

REFERENCES

Aléon J., Krot A. N., and McKeegan K. D. 2002. Calcium-aluminum-rich inclusions and amoeboid olivine aggregates from the CR carbonaceous chondrites. *Meteoritics & Planetary Science* 37: 1729–1755.

Anders E. and Grevesse N. 1989. Abundances of elements: Meteoritic and solar. *Geochimica et Cosmochimica Acta* 51: 197–214.

Beckett J. R., Spivack A. J., Hutcheon I. D., Wasserburg G. J., and Stopler E. M. 1990. Crystal chemical effects on the partitioning of trace elements between mineral and melt: An experimental study of melilite with application to refractory inclusions from carbonaceous chondrites. *Geochimica et Cosmochimica Acta* 54: 1755–1774.

Benstock E. J., Buseck P. R., and Steele I. M. 1997. Cathodoluminescence of meteoritic and synthetic forsterites at 296 and 77 K using TEM. *American Mineralogist* 82:310–315.

Chizmadia L. J., Rubin A. E., and Wasson J. T. 2002. Mineralogy and petrology of amoeboid olivine inclusions in CO3 chondrites: Relationship to parent-body aqueous alteration. *Meteoritics & Planetary Science* 37:1781–1796.

Coogan L. A., Hain A., Stahl S., and Chakraborty S. 2005. Experimental determination of the diffusion coefficient for calcium in olivine between 900 °C and 1500 °C. *Geochimica et Cosmochimica Acta* 69:3684–3694.

Davis A. M., Simon S. B., and Grossman L. 1992. Melilite composition trends during crystallization of Allende Type B1 refractory inclusion melts (abstract). 28th Lunar and Planetary Science Conference. pp. 281–282.

Dodson M. H. 1973. Closure temperature in cooling geochronological and petrological systems. *Contributions to Mineralogy and Petrology* 40:259–274.

Dominik C., Blum J., Cuzzi J. N., and Wurm G. 2006. Growth of dust as the initial step toward planet formation. In *Protostars and planets V*, edited by Reipurth B., Juwitt D., and Keil K. Tucson: The University of Arizona Press. pp. 783–800.

Fagan T. J., Krot A. N., Keil K., and Yurimoto H. 2004. Oxygen isotopic evolution of amoeboid olivine aggregates in the reduced CV3 chondrites Efremovka, Vigarano, and Leoville. *Geochimica et Cosmochimica Acta* 68:2591–2611.

Feigelson E., Townsley L., Gudel M., and Stassun K. 2006. X-ray properties of young stars and stellar clusters. In *Protostars and planets V*, edited by Reipurth B., Juwitt D., and Keil K. Tucson: The University of Arizona Press. pp. 313–328.

Grossman J. N. and Brearley A. J. 2005. The onset of metamorphism in ordinary and carbonaceous chondrites. *Meteoritics & Planetary Science* 40:87–122.

Hain A. 1998. ^{42}Ca Tracer diffusion in Olivin in Abhängigkeit von der Temperatur, dem Sauerstoffpartialdruck und der chemischen Zusammensetzung, Ph.D. thesis, Fachbereich Chemie der Justus Liebig Universität Gieβen, Gieβen, Germany.

Hiyagon H. and Hashimoto A. 1999. ^{16}O excesses in olivine inclusions in Yamato-86009 and Murchison chondrites and their relation to CAIs. *Science* 283:828–831.

Imae N., Tsuchiyama A., and Kitamura M. 1993. An experimental study of enstatite formation reaction between forsterite and Si-rich gas. *Earth and Planetary Science Letters* 118:21–30.

Ito M. and Ganguly J. 2006. Diffusion kinetics of Cr in olivine and ^{53}Mn-^{53}Cr thermo-chronology of early solar system objects. *Geochimica et Cosmochimica Acta* 70:799–809.

Itoh S., Russell S. S., and Yurimoto H. 2007. Oxygen and magnesium isotopic compositions of amoeboid olivine aggregates from the Semarkona LL3.0 chondrite. *Meteoritics & Planetary Science* 42:1241–1247.

Jones R. H. and Lofgren G. E. 1993. A comparison of FeO-rich, porphyritic olivine chondrules in unequilibrated chondrites and experimental analogues. *Meteoritics* 28:213–221.

Jurewicz A. J. G. and Watson E. B. 1988. Cations in olivine. Part 2: Diffusion in olivine xenocrysts with applications to petrology and mineral physics. *Contributions to Mineralogy and Petrology* 99:186–201.

Kimura M., Grossman J. N., and Weisberg M. K. 2008. Fe-Ni metal in primitive chondrites: Indicators of classification and metamorphic conditions for ordinary and CO chondrites. *Meteoritics & Planetary Science* 43:1161–1177.

Klock W., Thomas K. L., McKay D. S., and Palme H. 1989. Unusual olivine and pyroxene composition in interplanetary dust and unequilibrated ordinary chondrites. *Nature* 339:126–128.

Komatsu M., Krot A. N., Petaev M. I., Ulyanov A. A., Keil K., and Miyamoto M. 2001. Mineralogy and petrography of amoeboid olivine aggregates from the reduced CV3 chondrites Efremovka, Leoville, and Vigarano: Products of nebular condensation, accretion and annealing. *Meteoritics & Planetary Science* 36: 629–641.

Kozasa T. and Hasegawa H. 1987. Grain formation through nucleation process in astrophysical environments. *Progress of Theoretical Physics* 77:1402–1410.

Krauss O. and Wurm G. 2005. Photophoresis and the pileup of dust in young circumstellar disks. *The Astrophysical Journal* 630: 1088–1092.

Krot A. N., Petaev M. I., and Yurimoto H. 2004a. Amoeboid olivine aggregates with low-Ca pyroxenes: A genetic link between refractory inclusions and chondrules? *Geochimica et Cosmochimica Acta* 68:1923–1941.

Krot A. N., Fagan T. J., Keil K., McKeegan K. D., Sahijpal S.,

Hutcheon I. D., Petaev M. I., and Yurimoto H. 2004b. Ca, Al-rich inclusions, amoeboid olivine aggregates, and Al-rich chondrules from the unique carbonaceous chondrites Acfer 094: I. Mineralogy and petrology. *Geochimica et Cosmochimica Acta* 68:2167–2184.

Krot A. N., Petaev M. I., Russell S. S., Itoh S., Fagan T. J., Yurimoto H., Chizmadia L., Weisberg M. K., Komatsu M., Ulyanov A. A., and Keil K. 2004c. Amoeboid olivine aggregates and related objects in carbonaceous chondrites: Record of nebular and asteroid processes. *Chemie der Erde* 64:185–239.

Krot A. N., Fagan T. J., Nagashima K., Petaev M. I., and Yurimoto H. 2005. Origin of low-Ca pyroxene in amoeboid olivine aggregates: Evidence from oxygen isotope compositions. *Geochimica et Cosmochimica Acta* 69:1873–1881.

Kunihiro T., Nagashima K., and Yurimoto H. 2005. Microscopic oxygen isotopic homogeneity/heterogeneity in the matrix of Vigarano CV3 chondrite. *Geochimica et Cosmochimica Acta* 69: 763–773.

MacPherson G. J., Paque J. M., Stolper E., and Grossman L. 1984. The origin and significance of reverse zoning in melilite from Allende type B inclusions. *Journal of Geology* 92:289–305.

McDonnell R. D., Spiers C. J., and Peach C. J. 2002. Fabrication of dense forsterite-enstatite polycrystals for experimental studies. *Physics and Chemistry of Minerals* 29:19–31.

Morioka M. 1981. Cation diffusion in olivine-II. Ni-Mg, Mn-Mg, Mg and Ca. *Geochimica et Cosmochimica Acta* 45:1573–1580.

Nakagawa Y., Nakazawa K., and Hayashi C. 1981. Growth and sedimentation of dust grains in the primordial solar nebula. *Icarus* 45:517–528.

Pack A. and Palme H. 2003. Partitioning of Ca and Al between forsterite and silicate melt in dynamic systems with implications for the origin of Ca, Al-rich forsterites in primitive meteorites. *Meteoritics & Planetary Science* 38:1263–1281.

Pack A., Yurimoto H., and Palme H. 2004. Petrographic and oxygen-isotopic study of refractory forsterites from R-chondrite Dar al Gani 013 (R3.5–6), unequilibrated ordinary and carbonaceous chondrites. *Geochimica et Cosmochimica Acta* 68:1135–1157.

Petaev M. I. and Wood J. A. 2005. Meteoritic constraints on temperatures, pressures, cooling rates, chemical compositions, and modes of condensation in the solar nebula. In *Chondrites and the protoplanetary disk*, edited by Krot A. N., Scott E. R. D., and Reipurth B. Astronomical Society of the Pacific Conference Series. pp. 373–406.

Petaev M. I., Krot A. N., and Weisberg M. K. 2005. Chemistry of olivine in AOA's: Evidence for variable redox conditions in the solar nebula (abstract). *Meteoritics & Planetary Science* 40:A122.

Ryerson M. J., Durham W. B., Cherniak D. J., and Lanford W. A. 1989. Oxygen diffusion in olivine: Effect of oxygen fugacity and implications for creep. *Journal of Geophysical Research* 94:4105–4118.

Steele I. M. 1988. Mineralogy of meteorites revealed by cathodoluminescence. In *Spectroscopic characterization of minerals and their surfaces*, edited by Coyne L. M., McKeever S. W. S., and Blake D. F. American Chemical Society Symposium Series, vol. 415. Washington, D.C.:American Chemical Society. pp. 150–164.

Stolper E. 1982. Crystallization sequence of Ca-Al-rich inclusions from Allende: An experimental study. *Geochimica et Cosmochimica Acta* 46:2159–2180.

Sugiura N. and Krot A. N. 2007. ^{26}Al-^{26}Mg systematics of Ca-Al-rich inclusions, amoeboid olivine aggregates, and chondrules from the ungrouped carbonaceous chondrite Acfer 094. *Meteoritics & Planetary Science* 42:1183–1195.

Watanabe S., Nakagawa N., and Nakazawa K. 1990. Cooling and quasi-static contraction of the primitive solar nebula after gas accretion. *The Astrophysical Journal* 358:282–292.

Weisberg M. K., Connolly H. C. Jr., and Ebel D. S. 2004. Petrology and origin of amoeboid olivine aggregates in CR chondrites. *Meteoritics & Planetary Science* 39:1741–1753.

Weidenschilling S. J. 1984. Evolution of grains in a turbulent solar nebula. *Icarus* 60:553–567.

Wurm G. and Krauss O. 2006. Concentration and sorting of chondrules and CAIs in the late solar nebula. *Icarus* 180:487–495.